Journal of Solid State Chemistry **162,** 128–137 (2001)
doi:10.1006/jssc.2001.9372, available online at http://www.idealibrary.com on IDEAL®

Pseudo-One-Dimensional Periodic Domain Boundary Structures in Alkali Titanium Oxides

F. F. Xu,* Y. Bando,*,[1] K. Kurashima,* H. Ogawa,† and K. Inada‡

*Advanced Materials Laboratory, National Institute for Materials Science, 1-1 Namiki, Tsukuba, Ibaraki 305-0044, Japan; and ‡Otsuka Chemical Co., Ltd., 3-2-27 Ote Dori, Osaka 540-0021, Japan

Received May 30, 2001; in revised form August 13, 2001; accepted August 22, 2001

Potassium- and sodium-doped titanium (magnesium) oxides have been prepared from the starting powders of K_2O–$8TiO_2$–0.2MgO and a small amount of Na_2O. An interesting crystal structure has been discovered, namely the pseudo-one-dimensional periodic domain boundary structure with the average periodic value of $M = 3.3$. The domains show layered structures consisting of corrugated layers of $Ti(Mg)O_6$ octahedra, which could be either $Cs_x(Ti_{2-x/2}Mg_{x/2})O_4$-type or $K_x(Ti_{2-x/2}Mg_{x/2})O_4$-type orthorhombic crystal structure by different lattice displacement. These two phases employ disordered intergrowth rather than ordered intergrowth like in $Na_2Ti_7O_{15}$ which has a periodicity of $3 + 4 = 7$. Coherent domain boundaries were formed neglecting the crystal structures of domains. The formation of this periodic structure is believed to be related to the presence of a small amount of Mg and Na in the starting powders. Moreover, the accommodation of small Na cations caused the transformation of the crystal structure to be monoclinic with the space group $P2/m$. © 2001 Academic Press

Key Words: **domain boundary; one-dimensional periodic; alkali titanium oxides; electron microscopy; lepidocrocite-typed; transformation.**

1. INTRODUCTION

Some nonstoichiometric alkali titanium oxides show different layered structures which are related to the lepidocrocite γ-FeOOH-type structure by different lattice displacements. The structure consists of corrugated layers of edge- and corner-shared $Ti(Me)O_6$ octahedra. Figures 1a–1c show the crystal structures of the lepidocrocite γ-FeOOH (1), $Cs_x(Ti_{2-x/2}Mg_{x/2})O_4$ (CTMO) (2, 3), and $K_x(Ti_{2-x/2}Mg_{x/2})O_4$ (KTMO) (4) titanates. Alkali metals are incorporated into the interstices between the layers in order to compensate the charge balance which has been broken up by the partial replacement of Ti^{4+} by Mg^{2+}. Figure 1d illustrates the wavy ribbon of the layer extending along [100] direction in the CTMO and KTMO structures. In the CTMO structure, a reflection mirror exists on the alkali metal layer and alkali metals locate close to the body center of the cube composed of the eight coordinating oxygen ions. Thus the structure has the symmetry of the *Imm*2 space group. However, the space group changes to $Cmc2_1$ for the KTMO structure due to the existence of a $c/2$ glide plane. In this structure, alkali metals are coordinated to only seven oxygen atoms.

It has been reported that the $Cs_x(Ti_{2-x/2}Mg_{x/2})O_4$ structure can be interrupted periodically along the c-axis by a displacement of one octahedron in the b direction. This gives rise to enlarged unit cells and the symmetry changes to monoclinic as shown in Fig. 2. So far many composition-dependent long-periodic structures have been discovered. $K_2Ti_6O_{13}$ (5, 6) and $Na_2Ti_3O_7$ (7) consist of three octahedra along the long period. $K_2Ti_8O_{17}$ (8) and $K_3Ti_8O_{17}$ (9) exhibit four-octahedral periodicity while $Cs_2Ti_5O_{11}$ (10) shows five-octahedral periodicity. Meanwhile, ordered intergrowth of different crystal structures has been discovered which shows a polytypoid periodicity. For example, $Na_2Ti_7O_{15}$ (11), a product of ordered intergrowth of $Na_2Ti_6O_{13}$ and $Na_2Ti_8O_{17}$, has a periodicity of $3 + 4 = 7$, while $(A_2M_6O_{13})_n^* AM_4O_9$ (12), where $A = K$, Na, $M =$ Ti or Ti, Nb, $n = 1$, 2 or 3, exhibits a series of intergrowth phases with the possible periodicity of $3 + 2 = 5$, $3 + 3 + 2 = 8$, or $3 + 3 + 3 + 2 = 11$. Intergrowth variants consisting of more than five octahedra along the long period have not been discovered yet.

In our present study, sodium- and potassium-doped titanium oxides were prepared from starting powders of K_2O–$8TiO_2$–0.2MgO which contained impurity levels of Na_2O. An interesting structure is discovered in this material. It has a pseudo-one-dimensional periodic domain boundary structure along the c direction, with an average periodic value of $M = 3.3$, i.e., an average of 3.3 octahedra involved in the structure along the long period. The domain structure mimics that of CTMO, KTMO,

[1] To whom correspondence should be addressed. Fax: 81-298-516280. E-mail: bando.yoshio@momokusa.nims.go.jp.

0022-4596/01 $35.00

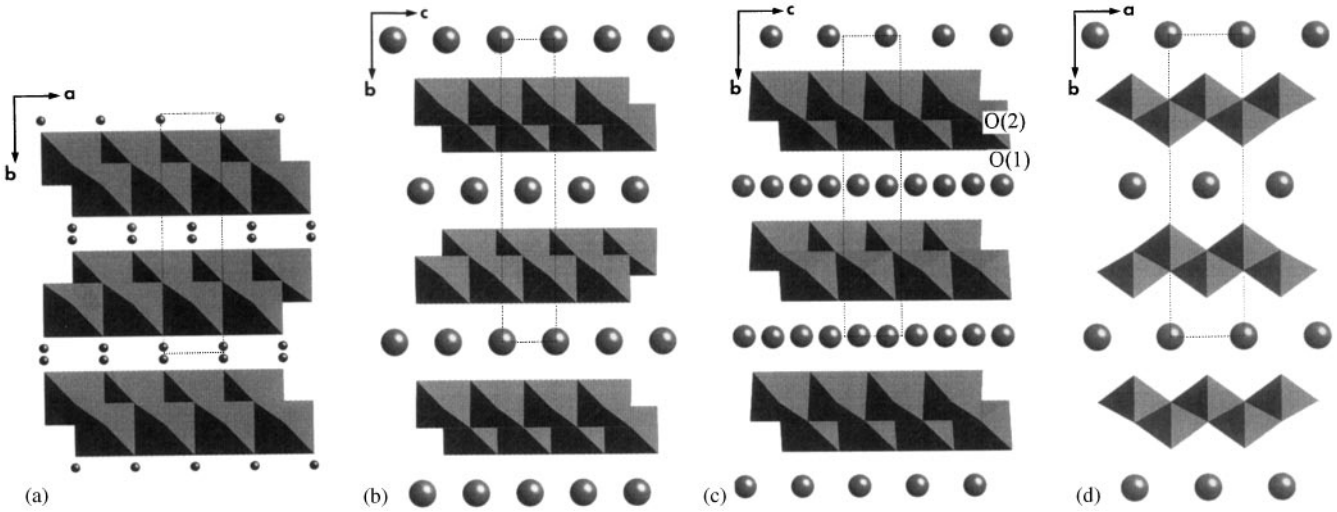

FIG. 1. Structures of (a) γ-FeOOH, (b) $Cs_x(Ti_{2-x/2}Mg_{x/2})O_4$, and (c) $K_x(Ti_{2-x/2}Mg_{x/2})O_4$, (d) shows the [001]-projected structure of $Cs_x(Ti_{2-x/2}Mg_{x/2})O_4$ and $K_x(Ti_{2-x/2}Mg_{x/2})O_4$.

$K_2Ti_6O_{13}$, or $K_2Ti_8O_{17}$ but employs disordered intergrowth rather than ordered configuration like in $Na_2Ti_7O_{15}$. In the present specimen, many domains show more or less deformed structures and the symmetry degrades to monoclinic with the space group $P2/m$ or $P2_1$. The formation of the periodic domain boundaries is believed to be related to the presence of small amounts of Mg and Na in the starting powder.

2. EXPERIMENTAL

The alkali titanium oxides samples were prepared from starting powders of K_2O–$8TiO_2$–0.2MgO. The mixed powders were then sintered at 1050°C for 4 hours in an electrical furnace. The as-sintered bulk material was smashed into powders. After postprocessing with H_2SO_4 and KOH solutions to remove the unreacted starting powders, the slurry was baked at 600°C for more than 3 hours. The eventual product was a fine white powder.

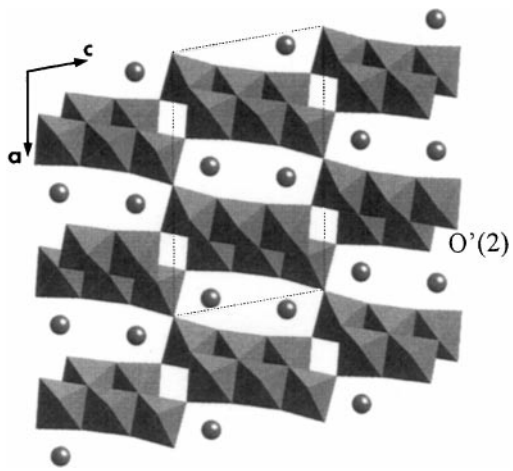

FIG. 2. Structure of $K_2Ti_6O_{13}$.

Since the crystals are plate-like, TEM observation from various crystal directions tends to be rather difficult. Therefore, the crystal powders were submerged into the Ni melts. The solidified bulk was then cut, ground, and polished to thin foils. The foils were eventually ion-milled until perforated.

TEM observations were performed using a field-emission transmission electron microscope (JEOL 3010F) equipped with an X-ray energy dispersive spectroscope (EDS). The microscope has an optimum spatial resolution of 0.14 nm and a spherical aberration coefficient *Cs* of 1.0 nm. Image simulation was performed by using the software of MacTempas (13).

3. RESULTS

3.1. General TEM Observation

The crystal fragments of the present alkali titanium oxides have a rectangular plate-like shape with average dimensions of 3 μm × 3 μm and a thickness of about 0.5 μm. The bright-field image and the schematic drawing of the crystal morphology are shown in Figs. 3a and 3b, respectively. It has been found that the crystals are severely faulted on the plane defined by the short dimension **b** and one of the long dimensions, i.e., **a**. Cleavage takes place normal to the fault plane.

Large numbers of diffraction patterns have been taken down the plane-view direction and both of the cross-sectional directions. Representative diffraction patterns are shown in Figs. 4 (plane-view direction) and 5 (Fig. 5a for

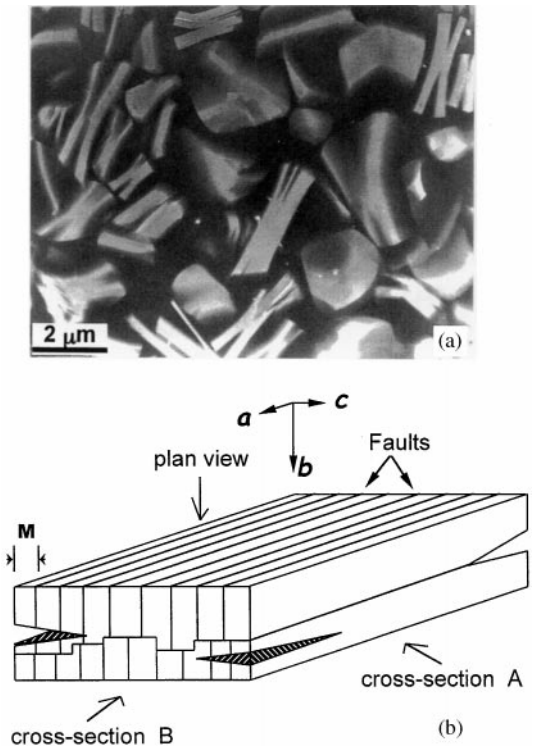

FIG. 3. (a) TEM bright-field image and (b) schematic drawing showing the typical morphology of the present alkali titanium oxides.

cross-section A and Fig. 5b for B as defined in Fig. 3b). The crystal fragments have uniform diffraction patterns in cross-sectional directions while the patterns from different fragments differ in plane-view direction.

The diffraction pattern shown in Fig. 5a is similar to the [001] pattern of CTMO and KTMO structures and to the [100] pattern of the long-periodic structures like $K_2Ti_6O_{13}$. The diffraction pattern in Fig. 5b is fairly complicated. However, the basic pattern consists of bright reflections similar to the [100] pattern of KTMO (see arrowed reflections). Although they are different, the diffraction patterns shown in Figs. 4a–4c have a basic rectangular sublattice (indicated in Fig. 4b) which is related either to the CTMO structure when an additional spot appears at the center of the rectangle, or to the KTMO structure if the additional spot is absent. Thus, analysis of diffraction patterns down various directions suggests that the crystal structure of our alkali titanates is basically a corrugated layered structure similar to those cited above.

Hereafter, the A direction indicated in Fig. 3b is projected parallel to the view direction of Fig. 1d while the B direction is the projection like those shown in Figs. 1b and 1c. In order to explicitly interpret this faulted structure, we temporarily define the three orthorhombic crystal dimensions, i.e., **a**, **b**, and **c**, as the same as those for the KTMO and CTMO structures (see Fig. 3b). The bold letters and indices in this paper and in the figures from Fig. 3 to Figs. 11a and 11b all refer to this definition of dimensions. It is seen that all the diffraction patterns show streaks along the **c** direction, indicating the presence of dense faults on the **c** plane.

3.2. Crystal Structures and Texture

It is noted that the diffraction spots shown in Fig. 5 are elongated and curved, characteristic of the reciprocal lattice from a mosaic microstructure. Figure 6a shows the dark-field (DF) image of an individual crystal fragment which is oriented close to the **a**-direction. A periodically parallel domain boundary structure is then revealed. The domains have nearly uniform size in width. The average span between the nearest two domain boundaries is only 1 nm. The domain boundary structure could be more clearly seen from the high-resolution images as shown in Fig. 6b, an **a**-projected lattice image, and in Fig. 6c, an (**a** + **b**)-projected image. The TEM observations discussed above suggest the domains are thin orthorhombic plates extending along the **a** and **b** directions and packing in the **c** direction. As clearly illustrated in the schematic drawing in Fig. 3b, the (001) interface involves the majority of the domain boundaries in this configuration. This means that the layered structure continues along the [100] "wave" direction of CTMO and KTMO but is interrupted periodically normal to the wave plane.

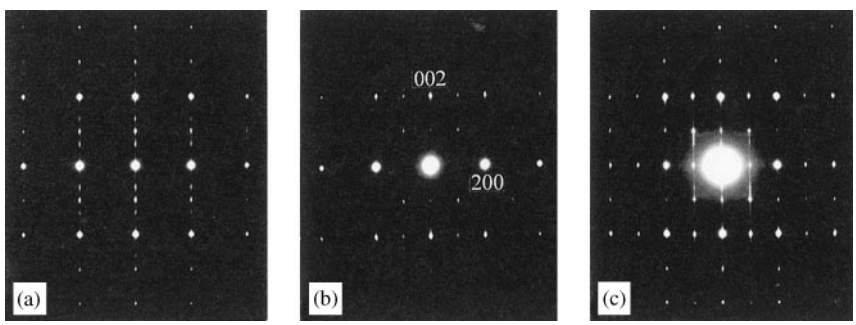

FIG. 4. Diffraction patterns in the plane-view direction. (a), (b), and (c) were obtained from different crystal fragments.

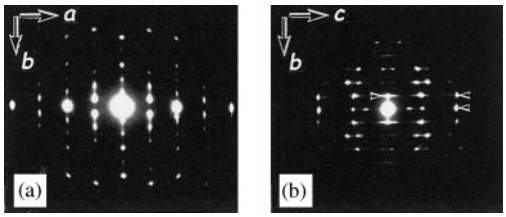

FIG. 5. Diffraction pattern in the direction of cross-section A (a) and of cross-section B (b) as defined in Fig. 3.

Figure 6b shows that between each two neighboring domains there is a lattice displacement, either upward or downward, of one octahedron in the **b** direction. The displacement vector is 10° to the paper normal in viewing Fig. 6c. The lattice shift is then fairly small in the direction normal to the **c** axis, i.e., about one-fifth of the interplanar distance in this view direction. Domain boundaries could be revealed via periodic contrast discontinuity. Octahedral layers are found to have tilted either clockwise or counterclockwise by a small angle in some domains. This is required for the formation of coherent interfaces between different domain structures as will be seen in the following.

3.2.1. *Pseudo-one-dimensional periodic domain boundaries.* In order to precisely determine the crystal structure of these nano-sized domains, image simulation is required. The computer-calculated images in the [100] projection are presented in Fig. 7a for the KTMO structure and in Fig. 7c for the CTMO structure. The **a**-projected HREM images of our sample are composed of arrays of bright and dark dots alternately packed along the **b** direction. In the present

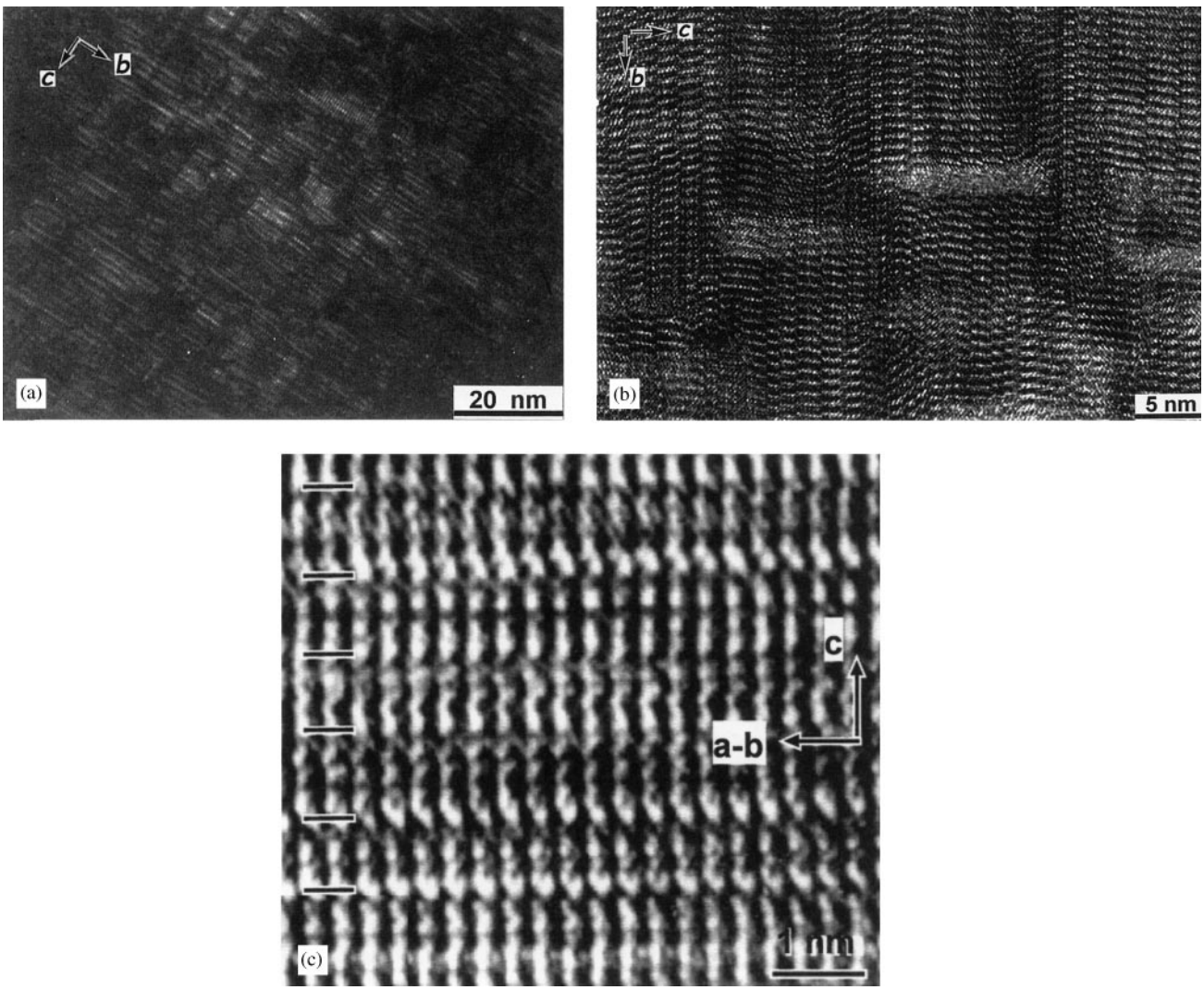

FIG. 6. (a) Dark-field image showing the periodic domain boundary structure. (b) and (c) are HREM images from **a** and (**a** + **b**) directions, respectively.

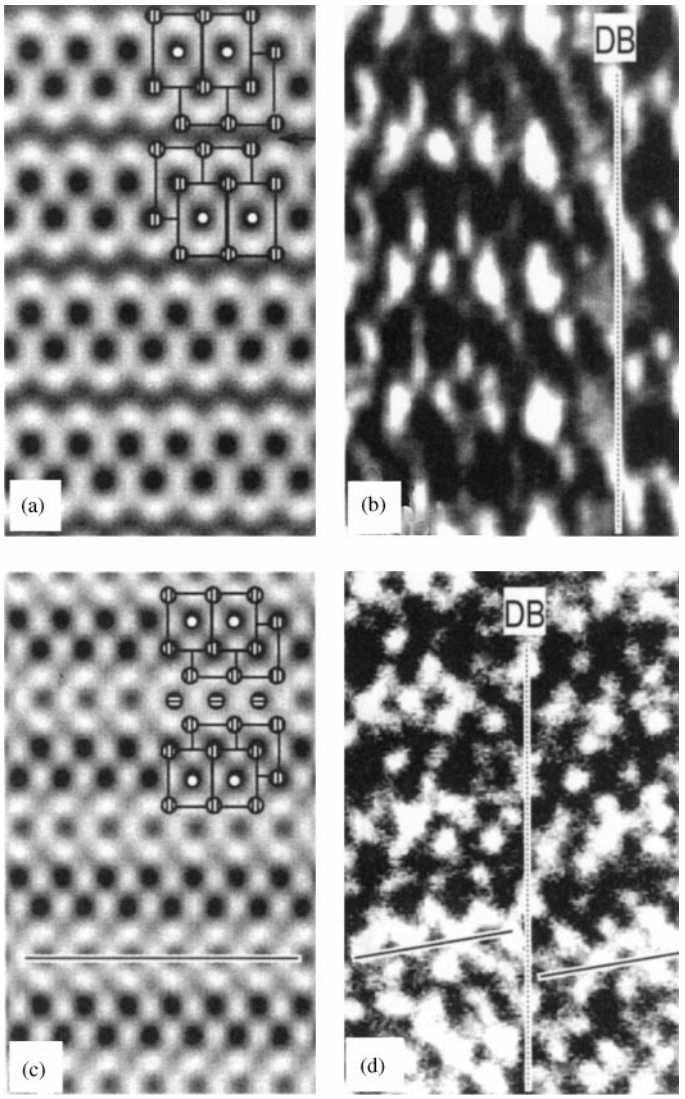

FIG. 7. Simulated images (a, c) and observed images (b, d) of $K_x(Ti_{2-x/2}Mg_{x/2})O_4$ (a, b) and $Cs_x(Ti_{2-x/2}Mg_{x/2})O_4$ (c, d). DB represents the domain boundary.

HREM images, the dark arrays are octahedral layers while bright arrays refer to the low-occupied interlayers. By comparing the simulated images to the observed micrographs, we find the coexistence of different crystal structures including KTMO (Fig. 7b) and CTMO (Fig. 7d). However, many domains slightly deviate from the orthorhombic symmetry as could be seen from Fig. 7b, where tiny deformations cause the dots on the image to be elongated.

In Fig. 7b the domain having the KTMO structure is bounded on the (001) plane with the neighboring domain. The octahedral layers are then normal to the domain boundaries. However, the layers are tilted by about 10° in the CTMO domains (Fig. 7d). The tilting angle differs slightly for the domains with deformed structures.

The tilted configuration is prerequisite to minimize the lattice misfit at the domain boundaries as could well be understood by structural modeling of interfaces shown in Fig. 8a. Figure 8a is a schematic drawing of the domain boundary structure in the present specimen based on the HREM observations. The period, i.e., the number of octahedra involved in the domain width, is arbitrarily defined in the drawing but matches the observed results which show random distribution of the domain width ranging between 2 to 7 octahedra (see Fig. 6b). In the present microstructure, three types of domain boundaries are discovered, i.e., boundaries between two CTMO domains (C–C), between a CTMO and a KTMO domain (C–K), and between two KTMO domains (K–K). It may be seen that coherent domain boundaries form via tilting of the CTMO domain when it connects to the (001) face of the KTMO domain. The octahedra are corner-linked at the C–K and K–K domain boundaries. However, both corner- and edge-shared octahedra are discovered at C–C domain boundaries. Extensive HREM observations suggest that the link type of the octahedra at domain boundaries seems to be related to the size of the domains on each side of the boundary. Small domains employ corner-sharing (see Fig. 10a) while edge-linked octahedra are always discovered at the domain boundaries between two large domains. The edge-linked domain boundary has a thickness of 1.5 octahedra (see dashed lines in Fig. 8a and Fig. 11a). It may be seen from Fig. 8a that among these different boundary configurations, the least deformation is required in forming the C–C domain boundary. The corner-linked C–C interface is similar to the structure in $K_2Ti_6O_{13}$ titanate as already shown in Fig. 2. The K–K interface is the most strained since the Ti–O bonds are largely shortened.

When the incident electron beams are parallel to the domain boundaries upon plane-view observation, the KTMO-type structure is [010]-projected while the CTMO structure is oriented close to the $[0\bar{1}1]$ projection. Since the *d*-spacing only differs by 0.06 Å between the (001) and the (011) interplanes, the superposition of the [010]- and $[0\bar{1}1]$-projected diffraction patterns causes the appearance of spots at the forbidden $\{001\}$ positions. They are actually $\{011\}$ diffraction spots as shown in Figs. 4b and 4c. This can be clearly seen in Fig. 9 where both the [010] diffraction pattern (Fig. 9a) of the KTMO structure and the $[0\bar{1}1]$ diffraction pattern (Fig. 9b) of the CTMO structure are illustrated. Therefore, the **b**-projected diffraction pattern (see Fig. 4) which shows bright spots at $\{001\}$ positions indicates that most domains have the CTMO structures in this selected region.

The present parallel-arrayed domain boundary structures are similar to the one-dimensional periodic antiphase boundary structures of CuAu II in which copper planes and gold planes of the $L1_0$ ordered fcc structure alternate every five unit cells along the *a* axis (14). This periodic superlattice

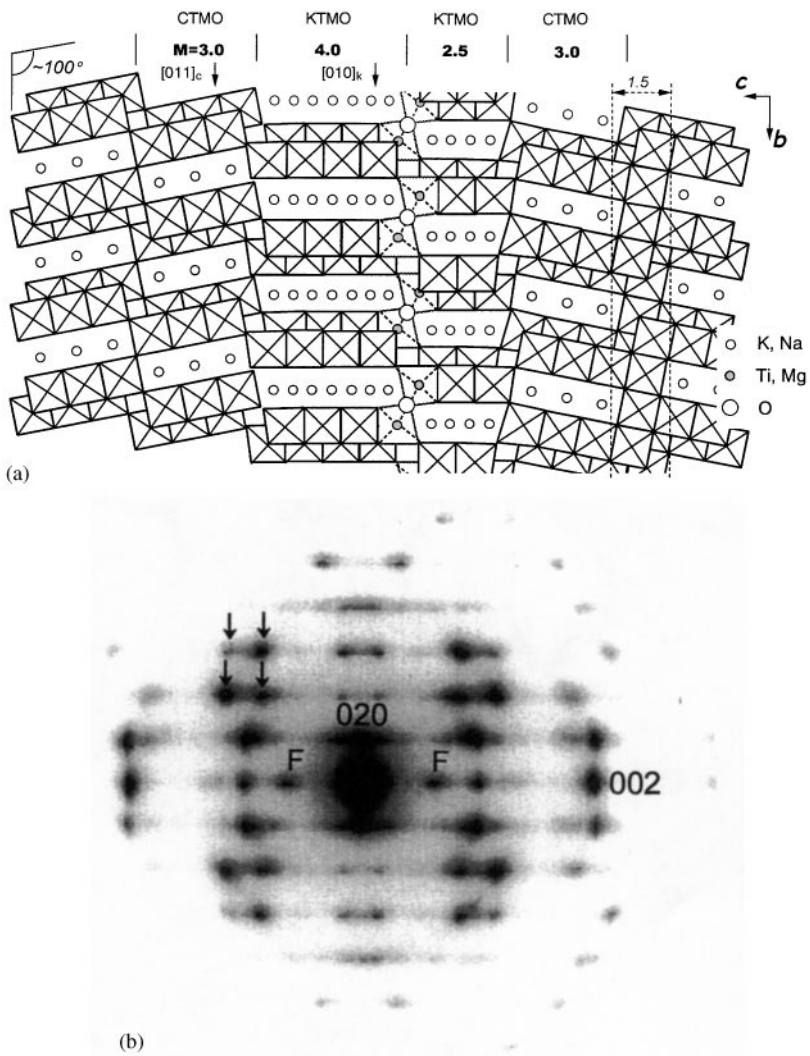

FIG. 8. Idealized structural model of the present pseudo-one-dimensional periodic domain boundary structure (a) and the interpretation of its diffraction pattern (b).

gives rise to antiphase domain boundaries on $\{100\}$ faces since the domains on each side of the boundary are identical except for a $\frac{1}{2}\langle 101\rangle$ lattice shift. However, in our case, the lattice displacement is not half the lattice vector. Therefore, we term the present structure as a pseudo-one-dimensional periodic domain boundary structure. Usually, this kind of periodic structure could be described by the periodic value M, i.e., the number of unit cells involved in the width of a domain between two neighboring domain boundaries. For the CuAu II periodic structure, the M value equals 5. The periodic value could be obtained either from the statistic measurements on the HREM images or from direct measurement on the diffraction patterns.

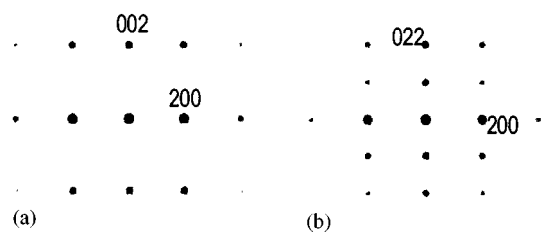

FIG. 9. Standard diffraction pattern of (a) KTMO structure in the [010] direction and (b) CTMO structure in the $[0\bar{1}1]$ direction.

The periodic boundary structures will lead to splitting of the diffraction spots in the direction normal to the domain boundaries. The separation of the two split spots in the reciprocal lattice indicates the average width of the domains in the real space. Figure 8b illustrates the magnified negative of the **a**-projected diffraction pattern. Part of the pattern could be indexed by the KTMO crystal structure. The faint "F" spots arise from the width ($\sim$1.5 octahedra) of the edge-linked C–C domain boundaries. The diffraction

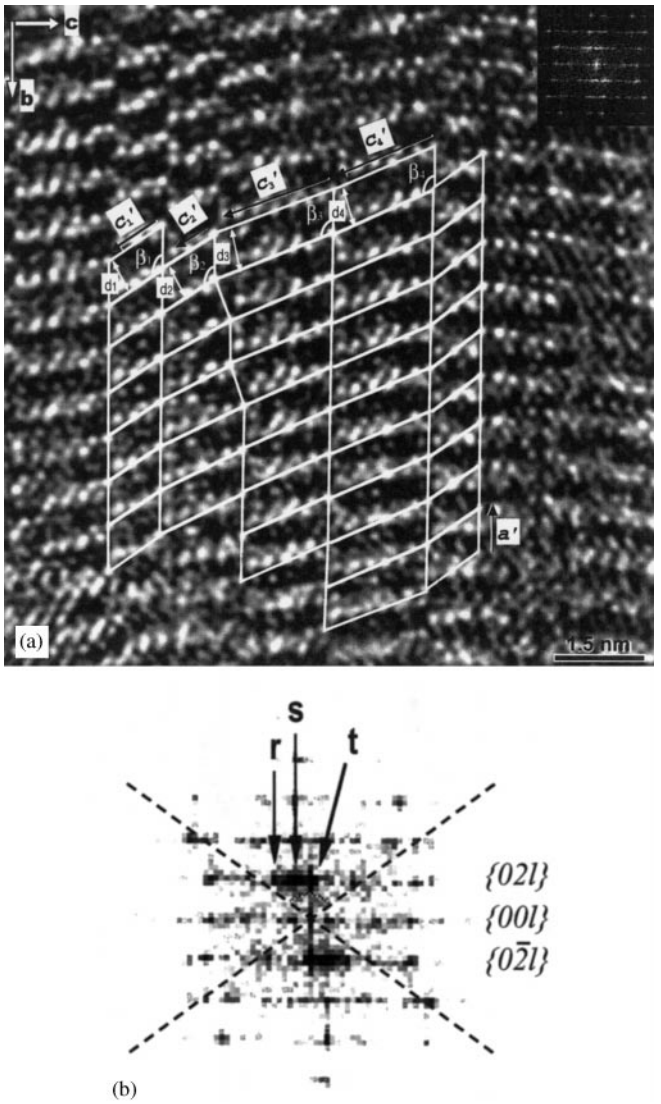

FIG. 10. Interpretation of splitting of diffraction spots for the present periodic domain boundary structure. (a) outlines the existence of supercells of which the effect on the diffraction pattern is illustrated in (b), an FFT diffractogram calculated from the image in (a).

pattern in Fig. 8b shows some extra reflections around the primary diffraction sites. These spots (indicated by pairs of arrows) are produced by splitting from the initial spots, e.g., (040), (060), (140), etc., owing to the presence of domain boundaries.

In the mosaic structure as shown in Fig. 10a, each column of the domain (CTMO) can be regarded as one-dimensional alignment along the **b** direction of a large monoclinic supercell. The grids of supercells projecting along their [010] direction are attached in Fig. 10a in which the basic dimensions are indicated by a' and c'_i for each column of monoclinic supercells. The β angle for each supercell is also indicated in the figure. These monoclinic supercells have identical a' and b' dimensions and differ only in the c' dimension. It can be seen that the β angle depends on the c'-dimension of the supercell. A small c' dimension will give a large β angle. Though the c' dimension and β angle might be different which results in different interplanar distances that are proportional to $\cos\beta$, e.g., $d_3 > d_4 > d_2 = d_1$ in Fig. 10a, $d/\cos\beta$ is a constant and equal to the (010) interplanar distance in the KTMO structure. Therefore, the reflections of the a' plane from different supercells all locate on the $\{0kl\}$ reflection lines of the KTMO structure with an individual $k = 2n$ as illustrated in Fig. 10b though crystal structures and orientations are different among KTMO, CTMO, and the deformed structure. Figure 10b is an enlarged fast Fourier-transformed diffractogram calculated from the region shown in Fig. 10a. In this diffractogram, the reflections indicated by arrow "r" refer to the small interplanar distances, e.g., d_1 and d_2, and large β angles, e.g., β_1 and β_2. However, for the larger supercells with decreased β angles, the reflections of a' faces get closer to the center of the diffraction pattern. The reflections marked by arrow "s" refer to the larger interplanar distances of d_3 and d_4. Reflections marked by arrow "t" come from the $(\bar{1}01)$ planes of those supercells. The $(\bar{1}01)$ planes from different supercells differ slightly both in orientation and in interplanar distance.

Kinetically, there exists an angular range of reflections similar to the texture structure. The small angle refers to a large c' dimension, i.e., a large M value. However, for a mosaic structure, there may be an effect known as secondary extinction associated with the repeated diffraction of an incident beam by several separate mosaic domains. The intensity incident upon one mosaic domain may be attenuated by diffraction in several previous domains having almost the same orientation. This effect will be most pronounced for inner reflections, for which the angular range of reflections from a small volume is greater (15). Such an effect upon a periodic domain boundary structure will give rise to splitting of reflections, the span of which refers to the average domain width.

The average width of the domain for the present titanium oxide crystal is estimated to be 0.98 nm from direct measurement of the span of the split spots in Fig. 5b. This width corresponds to the average periodic value $M = 3.3$, i.e., the domain structure contains an average of 3.3 octahedra along its width. The existence of reflection streaks intersecting the pairs of splitting spots indicates the presence of long-range ordered domains, i.e., a comparatively large area of single crystal structure in the present case as illustrated in Fig. 11a. The M value measured from the diffraction pattern matches the statistic analysis on the HREM images. On the diffraction pattern (Fig. 5b), a gradual decrease of the span is observed outward from the (000) spot probably due to the curved and elongated diffraction rods in the reciprocal lattice for this periodic mosaic structure.

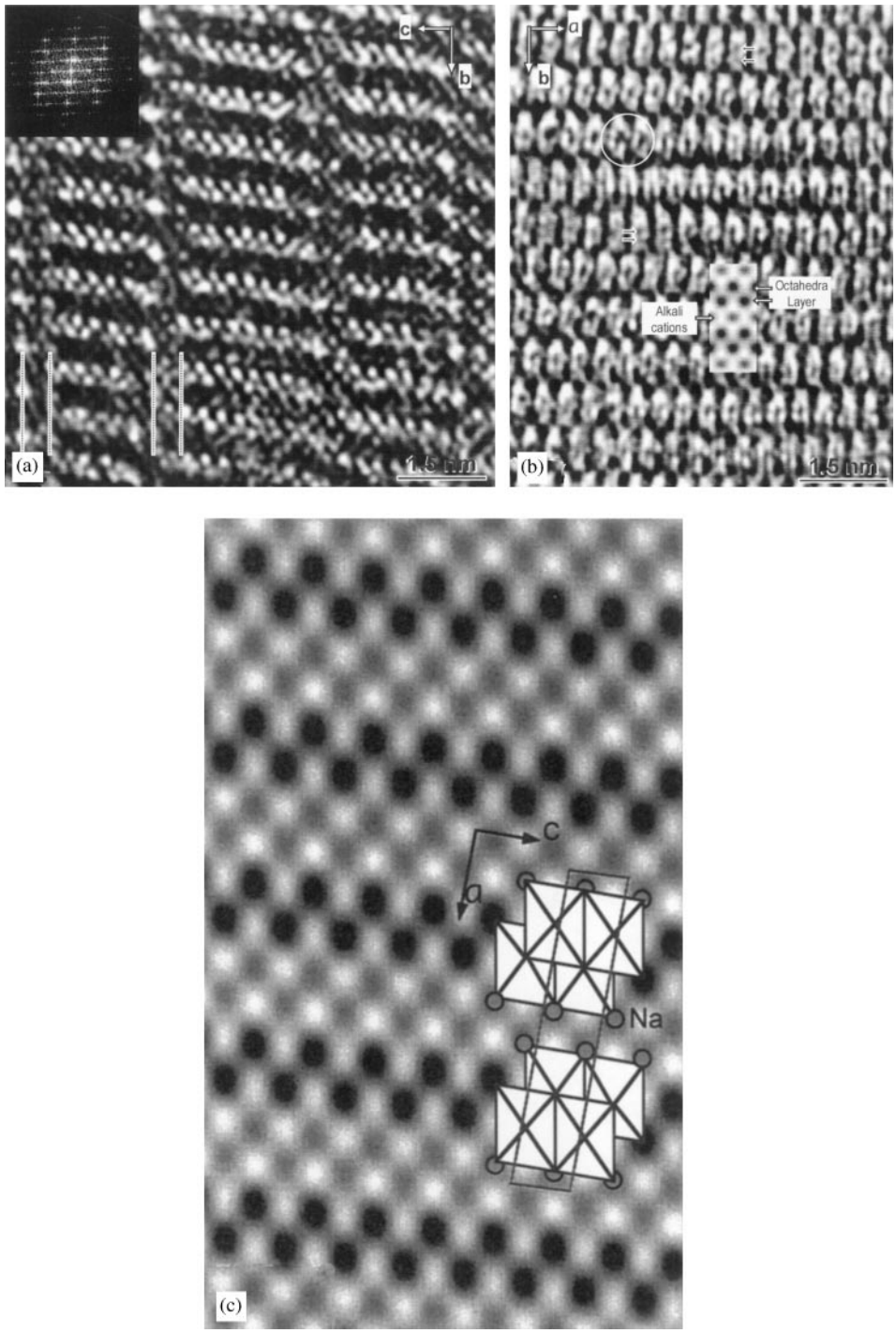

FIG. 11. HREM images from (a) **a** direction and (b) **c** direction showing the deformed crystal structure owing to the incorporation of small Na atoms. (c) shows a [010]-simulated image calculated from the proposed $P2/m$ structural model as attached on the figure.

3.2.2. *Structural transformation from orthorhombic to monoclinic*. TEM observations reveal the presence of slightly deformed crystal structures in the strained periodic domain boundary structure of our samples. Figure 11a shows the **a**-projected HREM image of the region containing the deformed structure. It can be seen that the corrugated octahedral-layered configuration is sustained but the neighboring layers have displaced by different distances of other than one or half the lattice vector and the octahedra themselves have deformed, i.e., deviating from

a rigid symmetric one by a shear parallel to the octahedral layer plane. In this configuration, the symmetric elements vanish in the **b** and **c** directions. The HREM image (Fig. 11b) viewed from the **c** direction reveals a different arrangement of alkali cations at the interlayers. Noting the double dark dots and rod-like dark dots (marked by arrows) at the interlayers other than a single round dot for both KTMO and CTMO structures (see the attached simulated image), we find that the y coordination varies for the alkali cations within the interlayer. However, a mirror plane remains normal to the octahedral layers. Therefore, by combining the information from these two differently oriented structural images, we can build the crystal structure for this deformed structure. The structure has a two-fold axis in the **a** direction with a mirror plane normal to it. The space group could be $P2/m$. Thus, the orthorhombic crystal has been transformed to the monoclinic structure. The β angle is found to be close to 90°. The lattice parameters could be derived from both the HREM image and diffraction pattern (Fig. 4c) and give $a = 15.47$, $b = 3.82$, $c = 3.10$ Å and $\beta \approx 91°$. Figure 11c illustrates the calculated image from a proposed $P2/m$ structural model which is shown in the figure. It is noted that the simulated image matches well with the observed micrograph in Fig. 11a. In the periodic domain boundary structure, the orientation relationships between the orthorhombic CTMO (o) and the monoclinic structure (m) are $[010]_o//[100]_m$, $[100]_o//[010]_m$, and $[001]_o \sim 1°$ to $[001]_m$. Since no conditions are available to limit the reflections for the $P2/m$ structure, this shows the appearance of reflections at the $(100)_o/(010)_m$ and $(hkl)_o/(hkl)_m$ $(h + k + l = 2n + 1)$ positions on the diffraction pattern shown in Fig. 4c. Figure 4b shows the diffraction spots at the $(hkl)_o/(hkl)_m$ $(h + k + l = 2n + 1)$ positions while the reflection is forbidden at the $(100)_o$ or $(010)_m$ site. Such extinction might be in agreement with a $P2_1/m$ or a $P2_1$ space group. This means the presence of a b-glide plane in the monoclinic structure probably arising from the fact that the incorporated alkali cations do not locate coplanarly on the (010) plane. The tendency of this configuration is revealed in Fig. 11b as indicated by circles.

Selected area diffraction (SAD) and EDS microanalyses have found that the crystal structures largely depend on the compositions. Table 1 presents the compositions of the crystals represented by each of the diffraction patterns shown in Fig. 4. The analysis region was identical for SAD and EDS performance. Figure 4a refers to the crystal composition of high K/Ti ratio. The diffraction pattern reveals a three-fold superstructure along the **c** direction which is similar to the crystal structure of $K_2Ti_6O_{13}$. Thus this region contains an almost perfect superlattice of which an example has been shown in Fig. 6c. Figure 4b and 4c refer to the crystal fragments having a very small amount of alkali metals accommodated in the crystal structure. These regions then possess a large area of nonstoichiometric titanium oxides or in other words, the number of domains is small in this selected region since the amount of the incorporated alkali atoms will increase with the formation of domain boundaries. An important difference in Na/K ratio should be noted between these two regions. It is found that the existence of sodium atoms will cause the appearance of some forbidden reflections. The higher the Na content, the more intense those reflections appear. It is then believed that the incorporation of these comparatively small sodium atoms will result in the deformation of crystal structure, i.e., from orthorhombic to monoclinic.

TABLE 1
Compositions of Crystal from Different Regions

Atomic ratio	Fig. 4a	Fig. 4b	Fig. 4c
Na:K:Mg:Ti	0.00:0.29:0.02:1.00	0.03:0.10:0.01:1.00	0.08:0.03:0.05:1.00

4. DISCUSSION

TEM analysis has discovered a pseudo-one-dimensional periodic domain boundary structure in the present alkali titanium oxides. Although the composition of the starting powders is close to the nominal composition of $K_2Ti_8O_{17}$ which has the uniform M value of 4, this phase could seldom be discovered. Instead, crystals contain mainly the short-range ordered domains which have an average width of 0.98 nm, i.e., the periodic value being $M = 3.3$. A lower M value than expected is probably due to the washing treatment with H_2SO_4 and KOH solutions during the material preparation. This treatment may have removed some of the potassium cations.

It could be found that the density of domain boundary is proportional to the alkali/Ti ratio in the starting powders. In the lepidocrocite-type octahedral layers, the coordination number of Ti atoms is 6 while O atoms have two different coordination numbers, i.e., 4 for O(2) and 2 for O(1). Upon the formation of domain boundaries, two 4-coordinated O(2) atoms (marked as O′(2) in Fig. 2) become 3-coordinated at each step of the layer. Therefore, two alkali cations are introduced. Meanwhile, the partial replacement of Ti^{4+} by Mg^{2+} also requires the accommodation of alkali cations to compensate the charge balance. The latter situation spoils the otherwise uniform periodic configuration of the nominal $K_2Ti_8O_{17}$ supercells. Instead, pseudo-one-dimensional periodic structures are formed. Due to the uneven distribution of alkali cations and magnesium ions, the crystal structures at different sites might apply to either KTMO or CTMO structure. Intergrowth of different periodic structures, e.g., $K_2Ti_6O_{13}$ and $K_2Ti_8O_{17}$, is discovered in the present specimen but ordering of intergrowth never occurred, leading to random distribution of domain width

rather than a fixed polytypoid periodicity like $3 + 4 = 7$ in $Na_2Ti_7O_{15}$ (11). This made the present diffraction pattern show split spots rather than superlattice reflections as for those ordered periodic structures of titanates.

Since the present layered structure is (only) stabilized by the alkali cations located at the interlayers, the crystal structure is strongly dependent on the atomic size and the bonding character of the incorporated alkali cations. The presence of a small amount of sodium ions has been found to cause the deformation of the crystal structure. This is due to the short Na–O bond length (2.31 Å) compared to the bond length (2.66 Å) of K–O. Therefore, the coordination number of these alkali cations could be different depending on the atomic size. The large Cs cation has the highest coordinate number of 8 in the CTMO structure while the intermediate-sized K cation has seven nearest neighbors in the KTMO structure. A Na-doped titanium oxide has been found to employ the lepidocrocite γ-FeOOH structure where small corrugated interlayer spaces are available and sodium ions are 6-coordinated (16). However, in the present material in which KTMO- and CTMO-type structures comprise the majority, sodium ions are not stable within such large interplanar spaces. In order for the Na cations to be as fully bonded as possible, the interlayers have to either approach or shift. The tilting as shown in the schematic diagram in Fig. 8a shortens the interlayer distance. This is why sodium cations are usually discovered in these domains. The Na–O bonding conditions could be satisfied via a $P2/m$ configuration as shown in Fig. 11c. In this structure, Na coordinates with two O(1) and two O(2) on the one side of the interlayer and two O(1) on the other side. TEM observations only discovered the sodium–potassium coexistent crystal structure but never the pure sodium titanium oxides since no lepidocrocite γ-FeOOH structure has been formed in the present material.

5. CONCLUSION

A periodic domain boundary structure has been observed in the present potassium–sodium-doped titanium (magnesium) oxides. The domains may apply to either KTMO- or CTMO-type layered structures of $Ti(Mg)O_6$ octahedra. The domain boundaries are formed by a lattice displacement of one octahedron normal to the layer, upon which the neighboring layers are linked by corner or edge sharing to form stepped ribbons. Intergrowth of different crystal structures, e.g., $K_2Ti_6O_{13}$ and $K_2Ti_8O_{17}$, is observed in the present specimen but ordering of intergrowth never occurred, which leads to random distribution of domain width rather than a fixed polytypoid periodicity like $3 + 4 = 7$ in $Na_2Ti_7O_{15}$. The average periodic value M is measured to be 3.3 for the present titanium oxides. The formation of coherent periodic domain boundary structure rather than the nominal $K_2Ti_8O_{17}$ crystal is believed to be related to the partial replacement of Ti by Mg. Meanwhile, the introduction of small Na cations has caused the crystal structure to transform from orthorhombic to monoclinic in which Na could be stabilized via 6-coordinated configuration.

ACKNOWLEDGMENTS

The authors are grateful to the reviewers for the precious revisions and comments. F.F.X. thanks the Japanese Science and Technology Agency for support.

REFERENCES

1. H. Christensen and A. N. Christensen, *Acta Chem. Scand. A* **32,** 87–88 (1978).
2. A. F. Reid, W. G. Mumme, and A. D. Wadsley, *Acta Crystallogr. B* **24,** 1228–1233 (1968).
3. W. A. England, J. E. Birkett, J. B. Goodenough, and P. J. Wiseman, *J. Solid State Chem.* **49,** 300–308 (1983).
4. D. Groult, C. Mercey, and B. Raveau, *J. Solid State Chem.* **32,** 289–296 (1980).
5. S. Andersson and A. D. Wadsley, *Acta Crystallogr.* **15,** 194–201 (1962).
6. E. Andersen, I. Andersen, and E. Skou, *Solid State Ionics* **27,** 181–187 (1988).
7. S. Andersson and A. D. Wadsley, *Acta Crystallogr.* **14,** 1245–1249 (1961).
8. T. Sasaki and Y. Fujiki, *J. Solid State Chem.* **83,** 45–51 (1989).
9. J. A. Watts, *J. Solid State Chem.* **1,** 319–325 (1969).
10. J. Kwiatkowska, I. E. Grey, I. C. Madsen, and L. A. Bursill, *Acta Crystallogr. B* **43,** 258–265 (1987).
11. A. D. Wadsley and W. G. Mumme, *Acta Crystallogr. B* **24,** 392–396 (1968).
12. M. Hervieu, *Ann. Chim. Fr.* **4,** 339 (1979).
13. MacTempas software package, see www.totalresolution.com/MacTempas.html.
14. A. B. Glossop and D. W. Pashley, *Proc. Roy. Soc. A* **250,** 132–136 (1959).
15. J. M. Cowley, "Diffraction Physics." North-Holland/American Elsevier Press, Amsterdam, 1975.
16. P. Parant, R. Olazcuaga, M. Devalette, C. Fouassier, and P. Hagenmuller, *J. Solid State Chem.* **3,** 1–11 (1971).